Radiofluorinated Probe for PET Imaging of Fatty Acid Binding Protein 4 in Cancer

Takashi Temma, PhD[1†]*; Kantaro Nishigori, PhD[1]*; Satoru Onoe, MS[1]; Sotaro Sampei[1]; Ikuo Kimura, PhD[2, 3]; Masahiro Ono, PhD[1]; and Hideo Saji, PhD[1]

[1] Department of Patho-Functional Bioanalysis, Graduate School of Pharmaceutical Sciences, Kyoto University; 46-29 Yoshida Shimoadachi-cho, Sakyo-ku, Kyoto 606-8501, Japan

[2] Department of Applied Biological Science, Graduate School of Agriculture, Tokyo University of Agriculture and Technology; 3-5-8 Saiwai-cho, Fuchu-Shi, Tokyo 183-8509, Japan

[3] Department of Pharmacogenomics, Graduate School of Pharmaceutical Sciences, Kyoto University; 46-29 Yoshida Shimoadachi-cho, Sakyo-ku, Kyoto 606-8501, Japan

[†] Present address: Department of Investigative Radiology, National Cerebral and Cardiovascular Center Research Institute; 5-7-1 Fujishiro-dai, Suita, Osaka 565-8565, Japan

[*] T.T. and K.N. contributed equally to this manuscript

Address correspondence and reprint requests to:

Hideo Saji, PhD

Department of Patho-Functional Bioanalysis, Graduate School of Pharmaceutical Sciences, Kyoto University; 46-29 Yoshida Shimoadachi-cho, Sakyo-ku, Kyoto 606-8501, Japan

Tel: +81-75-753-4556, Fax: +81-75-753-4568

E-mail: hsaji@pharm.kyoto-u.ac.jp

Running Title: PET probe for fatty acid binding protein 4

Key Words:

Fatty acid binding protein 4, radiolabeled probe, positron emission tomography, PET, nuclear imaging

Abstract **297 / 300 words**

Introduction: Cancer-associated adipocytes metabolically interact with adjacent cancer cells to promote tumor proliferation and metastasis. Fatty acid binding protein 4 (FABP4) participates in this interaction, and is gathering attention as a therapeutic and diagnostic target. Positron emission tomography (PET) is a useful diagnostic method that enables noninvasive *in vivo* quantitative imaging of biofunctional molecules with probes labeled with positron-emitting radioisotopes. Here a novel ^{18}F labeled probe for PET FABP4 imaging developed through dedicated drug design from a radioiodinated probe we recently reported is evaluated *in vitro* and *in viv*o.

Methods: We designed the [^{18}F]-labeled FTAP1 and FTAP3 probe, composed of a single or triple oxyethylene linker and a triazolopyrimidine scaffold derived from a FABP4 inhibitor. FABP4 binding affinities for chemically synthesized FTAP1 and FTAP3 were measured using FABP4 and 8-anilino-1-naphthalene sulfonic acid. Cell membrane permeability was measured using a commercially available plate assay system. After radiosynthesis, [^{18}F]FTAP1 affinity and selectivity were evaluated using immobilized FABP3, FABP4, and FABP5. Cell uptake was investigated using differentiated adipocytes expressing FABP4 with inhibitor treatment. Following biodistribution studies in C6 glioblastoma-bearing mice, *ex vivo* autoradiography and immunohistochemistry were

performed using thin sliced tumor sections. PET/CT imaging was then performed on C6 tumor bearing mice.

Results: FTAP1 showed high FABP4 affinity (K_i= 68 ± 8.9 nM) and adequate cell permeability. [^{18}F]FTAP1 with ≥ 98% radiochemical purity was shown to selectively bind to FABP4 (16.3- and 9.3-fold higher than for FABP3 and FABP5, respectively). [^{18}F]FTAP1 was taken up by FABP4 expressing cells, and this uptake could be blocked by an inhibitor, indicating very low non-specific cell binding. [^{18}F]FTAP1 showed high tumor accumulation, which demonstrates its potential use for *in vivo* tumor PET imaging, and the intratumoral radioactivity distribution corresponded to the FABP4 expression profile.

Conclusion: [^{18}F]FTAP1 is a promising PET probe to target FABP4.

Introduction

According to a 2011 report [1], more than 500 million adults worldwide were recognized as obese. Obesity is a major concern because it represents an important risk factor for diabetes, hypertension and cardiovascular diseases. The impact of obesity on cancer survival has been also noted. Renehan *et al*. reported that an increase in body mass index is a risk factor for some cancers, including esophageal adenocarcinoma and thyroid cancers [2]. The systemic pharmacological effect of adipokines secreted by adipocytes as well as increased insulin levels are major mechanisms of obesity in cancer development. In addition, cancer-associated adipocytes (CAAs) play an important role in tumor progression [3, 4], as was indicated by *in vitro* and *in vivo* evidence showing that CAAs promote tumor cell survival, proliferation, differentiation and migration [4, 5]. Although the detailed mechanisms are not fully elucidated, the interaction of CAAs with tumor cells seems to depend on biologically active substances such as interleukin 6 (IL-6) and free fatty acids [4].

Fatty acid binding proteins (FABPs) regulate lipid responses in cells and are involved in metabolic and inflammatory pathways [6]. Through the transportation of lipids to specific cell components, FABPs regulate lipid usage in cells for storage, signaling and transcriptional regulation. Among the FABPs, FABP4 is the best-characterized isoform

and is predominantly expressed in adipocytes and macrophages [6]. FABP4 regulates the activities of Jun *N*-terminal kinase (JNK) 1 to enhance production of cytokines such as tumor necrosis factor α (TNF-α), IL-1β, and monocyte chemoattractant protein 1 (MCP-1) [7, 8]. CAAs were recently reported to interact metabolically with cancer cells through the transport of free fatty acids on the cellular boundary, and this interaction could be inhibited by treatment of cells with a FABP4 selective inhibitor [5]. Furthermore, tumor proliferation and metastasis were significantly diminished in FABP4-knockout mice [5], indicating an important role for FABP4 in the metabolic interaction between CAAs and cancer cells as well as in tumor progression. Therefore, given the promise of FABP4 as a therapeutic target in such tumors, *in vivo* noninvasive imaging techniques are urgently needed for the development of therapeutic agents that target FABP4 and also to evaluate the functions of FABP4 in tumors.

We recently developed a FABP4 imaging probe, [$^{123/125}$I]TAP1, for use in nuclear imaging with single photon emission computed tomography (SPECT) [9]. Although the design of [$^{123/125}$I]TAP1 was based on the structures of selective FABP4 inhibitors and showed high affinity and selectivity for FABP4, this probe had high lipophilicity that caused significant nonspecific distribution *in vivo*. This lipophilicity was considered to be a limitation of this probe that required improvement before it could be used in

expanded *in vivo* imaging applications. Thus, we aimed to develop a FABP4 imaging probe that could be applied to *in vivo* FABP4 imaging in model mice using nuclear medical techniques. We describe the design of two candidate probes, [^{18}F]FTAP1 and [^{18}F]FTAP3 (Fig. 1), which are based on [^{123}I]TAP1. To reduce and optimize probe lipophilicity that will promote adequate intracellular targeting, we introduced radiofluorine (^{18}F) as the radioisotope for labeling for positron emission tomographic (PET) imaging at the same labeling position as in [$^{123/125}$I]TAP1 and introduced oxyethylene linkers with two different chain lengths for subtle lipophilicity control. We then synthesized and evaluated the usefulness of [^{18}F]FTAP1 and [^{18}F]FTAP3 *in vitro* and *in vivo*, and found that [^{18}F]FTAP1 is a promising FABP4 imaging probe.

Materials and Methods

1. General

All reagents were purchased from Nacalai Tesque, Inc. and Wakenyaku Co., Ltd., and were used without further purification unless otherwise noted. ^{1}H-NMR spectra were obtained at 400 MHz on JEOL JNM-AL400 NMR spectrometers at room temperature with tetramethylsilane (TMS) as an internal standard. Chemical shifts are reported as δ values (parts per million) relative to the TMS standard. Coupling constants are reported in Hertz. Multiplicity is defined by s (singlet), d (doublet), t (triplet), and m (multiplet). High resolution mass spectra (HRMS) were acquired on a JMS-SX 102A QQ or JMS-GC-mate mass spectrometer (JEOL). Recombinant hexahistidine (his)-tagged FABP3, FABP4 and FABP5 proteins were purchased from Cayman Chemical Company (Ann Arbor, MI, USA). All PET scans were obtained on a small-animal scanner (FX3300 imager; SII NanoTechnology Inc., Northridge, CA, USA).

2. Animals & Cells

Animal experiments were conducted in accordance with our institutional guidelines and approved by the Kyoto University Animal Care Committee (Permit Number: 2012-49, 2013-33). Male ddY mice and male Balb/c nu-nu mice (Japan SLC, Inc.) were fed

standard chow and had access to water *ad libitum*. All surgery was performed under isoflurane anesthesia, and all efforts were made to minimize suffering. Rat C6 glioma cells (Health Science Research Resources Bank) were cultured at 37 °C in 5% CO_2 in McCoy's 5A Modified Medium supplemented with 10% heat-inactivated fetal bovine serum (FBS, Nichirei Bioscience Inc.), 50 U/ml penicillin and 50 μg/ml streptomycin (Nacalai Tesque, Inc.). C6 cells were suspended in PBS(-) followed by subcutaneous inoculation into the right hind legs of Balb/c nu-nu mice (5×10^6 cells/100 μl). The animals were used for experiments 14 days after inoculation.

Murine 3T3-L1 preadipocytes (American Type Culture Collection) were cultured in Dulbecco's Modified Eagle Medium (DMEM, Nissui Pharmaceutical Co., Ltd.) supplemented with 10% heat-inactivated FBS, 50 U/ml penicillin and 50 μg/ml streptomycin at 37 °C in 5% CO_2. Differentiation of 3T3-L1 cells was performed as described previously [10]. Briefly, 2 days after confluence was reached, the medium was replaced with DMEM containing 10% FBS and inducers (0.25 mM dexamethasone, 10 μg/ml insulin, 0.5 mM 3-isobutyl-1-methylxanthine and 10 μM pioglitazone hydrochloride) for 2 days. The medium was then changed to DMEM supplemented with 10% FBS, 10 μg/ml insulin and 10 μM pioglitazone hydrochloride, and then incubated for 2 days. The medium was then changed every other day with DMEM supplemented

with 10% FBS and 10 μM pioglitazone hydrochloride. After 8-10 days, the differentiated adipocytes were confirmed by western blotting and Oil red O staining following our previous studies [9, 10] and used for experiments.

3. Chemistry

Nonradioactive FTAP1, nonradioactive FTAP3, and FTAP1 precursors were synthesized as shown in Fig. 1. In each step in general, the solvent was evaporated under reduced pressure after the reaction, water was added, and the product was extracted into ethyl acetate. After the organic layer was dried over Na_2SO_4 and filtered, the solvent was evaporated and the residue was purified by silica gel chromatography.

*5-(Chloromethyl)-2-phenyl-[1,2,4]triazolo[1,5-a]pyrimidin-7(4H)-one (**1**)*

Compound **1** was synthesized according to previously reported procedures [11].

*1-(Benzyloxy)-3-(2-fluoroethoxy)benzene (**2**)*

3-Benzyloxyphenol (0.9 g, 4.6 mmol) and 2-fluoroethyl 4-methylbenzenesulfonate (1.0 g, 4.6 mmol) were reacted overnight at 105 °C in the presence of K_2CO_3 (1.3 g, 9.2 mmol) in DMF (27 ml). Silica gel chromatography (ethyl acetate/hexane = 1/8) to yield

2 (0.9 g, 3.7 mmol, 80 % yield). ^{1}H NMR: ($CDCl_3$, 400 MHz) 7.44-7.31 (m, 5H), 7.21-7.17 (t, 1H, *J*=8.5 Hz), 6.63-6.53 (m, 3H), 5.05 (s, 2H), 4.81-4.67 (td, 2H, *J*=4.4, 47 Hz), 4.24-4.15 (td, 2H, *J*=4.4, 28 Hz).

*5-[{3-(2-Fluoroethoxy)phenoxy}methyl]2-phenyl-[1,2,4]triazolo[1,5-a]pyrimidin-7(4H)-one (**3**)*

A mixture of **2** (0.9 g, 3.7 mmol) and palladium carbon (Pd 10%, 0.1 g) was stirred in methanol (30 ml) at room temperature for 1 hr under a hydrogen atmosphere at atmospheric pressure. After filtration, the solvent was evaporated. The residue (0.7 g, 4.3 mmol) and **1** (0.8 g, 2.9 mmol) were then reacted in the presence of K_2CO_3 (1.2 g, 8.7 mmol) in DMF (45 ml) at 85 °C overnight. Silica gel chromatography ($CHCl_3$/methanol = 20/1) to yield **3** (nonradioactive FTAP1, 0.1 g, 0.3 mmol, 11 % yield). ^{1}H NMR: (DMSO-d_6, 400 MHz) 8.13-8.11 (d, 2H, *J*=8.2 Hz), 7.55-7.53 (m, 3H), 7.27-7.22 (t, 1H, *J*=8.0 Hz), 6.69-6.62 (m, 3H), 6.12 (s, 1H), 5.11 (s, 2H), 4.81-4.19 (m, 4H). HRMS (FAB+): the calculated m/z for $C_{20}H_{18}FN_4O_3$ was 381.1363, and the actual m/z was 381.1360.

*2-{2-(2-Fluoroethoxy)ethoxy}ethyl 4-methylbenzenesulfonate (**4**)*

Tetrabutylammonium fluoride (6.3 g, 24 mmol) was added to 1,2-bis[2-(*p*-toluenesulfonyloxy)ethoxy]ethane (1.0 g, 20 mmol) in THF (40 ml) at room temperature. The mixture was stirred at 85 °C for 8 hr. Silica gel chromatography (ethyl acetate/hexane = 1/2) to yield **4** (1.1 g, 3.6 mmol, 18 % yield). ^{1}H NMR: ($CDCl_3$, 400 MHz) 7.81-7.79 (d, 2H, *J*=7.8 Hz), 7.36-7.33 (d, 2H, *J*=8.7 Hz), 4.61-4.59 (t, 1H, *J*=4.1 Hz), 4.49-4.47 (t, 1H, *J*=4.1 Hz), 4.18-4.16 (t, 2H, *J*=4.8 Hz), 3.76-3.74 (t, 1H, *J*=4.1 Hz), 3.71-3.59 (m, 7H), 2.45 (s, 3H).

*1-(Benzyloxy)-3-[2-{2-(2-fluoroethoxy)ethoxy}ethoxy]benzene (**5**)*

3-Benzyloxyphenol (0.1 g, 0.7 mmol) and **4** (0.2 g, 0.7 mmol) were reacted in the presence of K_2CO_3 (0.2 g, 1.4 mmol) in DMF (5 ml) at 105 °C overnight. Silica gel chromatography (ethyl acetate/hexane = 1/3) to yield **5** (0.2 g, 0.5 mmol, 72 % yield). ^{1}H NMR: ($CDCl_3$, 400 MHz) 7.44-7.32 (m, 5H), 7.19-7.15 (t, 1H, *J*=8.0 Hz), 6.59-6.51 (m, 3H), 5.04 (s, 2H), 4.63-4.49 (m, 2H), 4.12-4.10 (t, 2H, *J*=4.3 Hz), 3.89-3.84 (t, 2H, *J*=5.0 Hz), 3.80-3.70 (m, 6H).

*5-[[3-[2-{2-(2-Fluoroethoxy)ethoxy)ethoxy}phenoxy]methyl]-2-phenyl-[1,2,4]triazolo[1,5-a]pyrimidin-7(4H)-one (**6**)*

A mixture of 5 (0.1 g, 0.70 mmol) and palladium carbon (Pd 10%, 0.01 g) was stirred in methanol (5 ml) at room temperature for 2 hr under a hydrogen atmosphere. After filtration, the solvent was evaporated. Then, the residue (0.04 g, 0.2 mmol) and **1** (0.03 g, 0.1 mmol) were reacted in the presence of K_2CO_3 (0.02 g, 0.16 mmol) in DMF (5 ml) at 85 °C for 5 hr. Silica gel chromatography ($CHCl_3$/methanol = 10/1) to yield **6** (nonradioactive FTAP3, 0.005 g, 0.01 mmol, 13 % yield). ^{1}H NMR: (DMSO-d_6, 400 MHz) 8.14-8.12 (d, 2H, *J*=7.3 Hz), 7.55-7.53 (m, 3H), 7.25-7.21 (t, 1H, *J*=8.0 Hz), 6.66-6.59 (m, 3H), 6.11 (s, 1H), 5.10 (s, 2H), 4.57-4.44 (m, 2H), 4.10-4.08 (t, 2H, *J*=4.4 Hz), 3.75-3.58 (m, 8H). HRMS (FAB+): the calculated m/z for $C_{24}H_{26}FN_4O_5$ was 469.1887, and the actual m/z was 469.1889.

2-{3-(Benzyloxy)phenoxy}ethanol (7)

3-Benzyloxyphenol (2.0 g, 10 mmol) and ethylene bromohydrin (3.8 g, 30 mmol) were reacted overnight in the presence of K_2CO_3 (4.1 g, 30 mmol) in DMF (70 ml) at 85 °C. Silica gel chromatography (ethyl acetate/hexane = 1/3) to yield **7** (1.7 g, 7.0 mmol, 70 % yield). ^{1}H NMR: ($CDCl_3$, 400 MHz) 7.44-7.33 (m, 5H), 7.21-7.17 (t, 1H, *J*=8.5 Hz), 6.62-6.52 (m, 3H), 5.05 (s, 2H), 4.07-4.05 (m, 2H), 3.97-3.93 (m, 2H).

*3-[2{(tert-Butyldimethylsilyl)oxy}ethoxy]phenol (**8**)*

Tert-butyldimethylsilyl chloride (1.7 g, 11.2 mmol) and imidazole (1.0 g, 15 mmol) were added to **7** (1.7 g, 7.0 mmol) in CH_2Cl_2 (20 ml) at 4 °C. The mixture was stirred at room temperature for 5 hr. Silica gel chromatography (ethyl acetate/hexane = 1/15) was performed. Then, the recovered sample (2.3 g, 6.5 mmol) and palladium carbon (Pd 10%, 0.2 g) was stirred in methanol (50 ml) at room temperature for 3 hr under a hydrogen atmosphere. After filtration, the solvent was evaporated and purified by silica gel chromatography (ethyl acetate/hexane = 1/8) to yield **8** (1.7 g, 6.3 mmol, 88 % yield). ^{1}H NMR: ($CDCl_3$, 400 MHz) 7.13-7.09 (t, 1H, *J*=8.5 Hz), 6.50-6.41 (m, 3H), 4.02-3.94 (m, 4H), 0.91 (s, 9H), 0.10 (s, 6H).

*5-[{3-(2-Hydroxyethoxy)phenoxy}methyl]-2-phenyl-[1,2,4]triazolo[1,5-a]pyrimidin-7(4H)-one (**9**)*

1 (0.6 g, 2.5 mmol) and **8** (1.0 g, 3.7 mmol) were reacted for 6 hr in the presence of K_2CO_3 (1.0 g, 7.5 mmol) in DMF (50 ml) at 85 °C. Silica gel chromatography ($CHCl_3$/methanol = 30/1) was performed. Tetrabutylammonium fluoride (0.3 g, 1.0 mmol) was added to the recovered sample (0.4 g, 0.8 mmol) in THF (15 ml) at 4 °C. The mixture was stirred at room temperature for 2 hr. Silica gel chromatography

($CHCl_3$/methanol = 10/1) to yield **9** (0.2 g, 0.5 mmol, 19 % yield). ^{1}H NMR: (DMSO-d_6, 400 MHz) 8.13-8.11 (dd, 2H, *J*=8.2, 1.4 Hz), 7.54-7.48 (m, 3H), 7.22-7.18 (t, 1H, *J*=8.7 Hz), 6.62-6.55 (m, 3H), 5.96 (s, 1H), 5.02 (s, 2H), 3.98-3.96 (t, 2H, *J*=4.8 Hz), 3.18-3.14 (m, 2H).

*2-[3-{(7-Oxo-2-phenyl-4,7-dihydro-[1,2,4]triazolo[1,5-a]pyrimidin-5-yl)methoxy}phenoxy]ethyl 4-methylbenzenesulfonate (**10**)*

p-Toluenesulfonyl chloride (0.1 g, 0.7 mmol), triethylamine (0.1 g, 1.0 mmol) and *N*,*N*-dimethyl-4-aminopyridine (0.006 g, 0.05 mmol) were added to **9** (0.2 g, 0.5 mmol) in CH_2Cl_2 (10 ml) at 4 °C. The mixture was stirred at room temperature for 6 hr. Silica gel chromatography ($CHCl_3$/methanol = 30/1) to yield **10** (FTAP1 precursor, 0.02 g, 0.04 mmol, 7.9 % yield). ^{1}H NMR: (DMSO-d_6, 400 MHz) 8.14-8.11 (d, 2H, *J*=10.1 Hz), 7.81-7.79 (d, 2H, *J*=8.2 Hz), 7.55-7.47 (m, 5H), 7.23-7.19 (t, 1H, *J*=7.8 Hz), 6.67-6.49 (m, 3H), 6.11 (s, 1H), 5.09 (s, 2H), 4.34-4.32 (m, 2H), 4.17-4.15 (m, 2H), 2.41 (s, 3H).

4. In vitro evaluation of nonradioactive compounds

The binding affinity of FTAP1 and FTAP3 for FABP4 was measured by competitive binding experiments using 8-anilino-1-naphthalene sulfonic acid (1,8-ANS) as the tracer

[12]. Briefly, a mixture containing 0.12 ml phosphate buffer (50 mM, pH = 7.4), 0.03 ml FTAP1 or FTAP3 (65 μM-4 nM) in DMSO, 0.075 ml 1,8-ANS (24 nM) in phosphate buffer (0.2% ethanol, v/v) and 0.075 ml FABP4 (1 μM) in phosphate buffer was incubated at room temperature for 5 min. The fluorescence intensity at an excitation and emission wavelength of 370 and 475 nm, respectively, was plotted, and values for the half-maximal inhibitory concentration (IC_{50}) were determined from displacement curves of three independent experiments using GraphPad Prism 5 (GraphPad Software, San Diego, CA). The inhibition constants (K_i) were calculated using the Cheng-Prusoff equation: $K_i = IC_{50}/(1+[L]/K_d)$, where [L] is the 1,8-ANS concentration and K_d is the 1,8-ANS dissociation constant. The K_d value of 1,8-ANS for FABP4 was previously calculated to be 1.2 μM [9].

The membrane permeability of FTAP1 and FTAP3 was measured using a pre-coated parallel artificial membrane permeation assay (PAMPA) plate system (BD Biosciences) following the manufacturer's procedures. Briefly, the test compounds (100-200 μM, 0.2 ml) were added to the donor plate and PBS (-) (0.2 ml) was added to the acceptor plate in the PAMPA plate assembly. After coupling both plates together and incubating at room temperature for 5 hr, 0.15 ml of the sample was obtained from each plate and 0.15 ml of the original compound solution was also obtained. Then, the absorbance of each sample

was measured at 280 nm. The permeability was calculated as: Pe (cm/s) = (-ln[1-$C_A/C_{equilibrium}$])/St $(1/V_D+1/V_A)$ and $C_{equilibrium} = [C_DV_D+C_AV_A]/(V_D+V_A)$. $C_D = C_0 (A_D-A_{buffer})/(A_0-A_{buffer})$ and $C_A = C_0 (A_A-A_{buffer})/(A_0-A_{buffer})$. C_0 is the concentration of the starting sample and A_0, A_{buffer}, A_D and A_A are absorbances of the starting sample, buffer, donor and acceptor, respectively. V_D and V_A are the donor and acceptor volumes, respectively. S is the membrane area and t is the incubation time.

5. Radiosynthesis of [^{18}F]FTAP1

[^{18}F]Fluoride was produced in a cyclotron, trapped on an anion exchange cartridge, and eluted with a K_2CO_3 solution (33 mM). Kryptofix$_{222}$ (20 mg) was dissolved in a solution of [^{18}F]fluoride in water. The solvent was then removed at 120 °C under a stream of nitrogen gas. The residue was azeotropically dried with 0.3 ml of anhydrous CH_3CN twice at 120 °C under a stream of nitrogen gas. A solution of the mesylate precursor **10** (2.0 mg) in DMSO (0.2 ml) was added to the reaction vessel and heated at 130 °C for 2 min under microwave (50W, SAIDA PMCR-50). After cooling to room temperature, the mixture was passed through a preconditioned Sep-Pak Plus C18 cartridge (Waters). The cartridge was washed with 20 ml water, and eluted with 3 ml CH_3CN. After the solvent was removed, the residue was dissolved in CH_3CN and subjected to RP-HPLC for

purification (Nacalai Tesque, 5C18-AR-II, 10 mm x 250 mm, CH_3CN/water = 50/50 (0 min)-70/30 (40 min); flow rate = 1.5 ml/min). Radiochemical purity of purified [^{18}F]FTAP1 was evaluated with another RP-HPLC analysis. The decay-uncorrected radiochemical yield of [^{18}F]FTAP1 from [^{18}F]KF was determined with a dose calibrator.

6. In vitro evaluation of [^{18}F]FTAP1

For protein immobilization, his-tagged FABP3 (0.75 mg/ml, 0.003 ml, 1.5 μg), FABP4 (0.75 mg/ml, 0.002 ml, 1.5 μg) and FABP5 (0.70 mg/ml, 0.002 ml, 1.4 μg) in 50 mM phosphate buffer containing 100 mM NaCl (20% glycerol, v/v, pH = 7.2) were incubated with 0.02 ml Ni-NTA Magnetic Agarose Beads (Qiagen) and 0.5 ml protein binding buffer (50 mM NaH_2PO_4, 300 mM NaCl, 10 mM imidazole, pH = 8.0) at room temperature for 1 hr following the manufacturer's procedures. After supernatant removal, protein binding buffer with 1% BSA was added, and incubated at room temperature for 30 min. After removal of the supernatant, 0.4 ml of interaction buffer (50 mM NaH_2PO_4, 300 mM NaCl, 10 mM imidazole, and 0.005% Tween, v/v, pH = 8.0) and 0.05 ml of interaction buffer including [^{18}F]FTAP1 (0.08 MBq, 5% ethanol, v/v) were added. For measurement of non-specific binding, 0.05 ml of nonradioactive FTAP1 in interaction buffer (5% ethanol, v/v, 1.1 μM) was added to [^{18}F]FTAP1. After incubation at room

temperature for 2 hr, the supernatants were removed, and the beads washed with interaction buffer (5% ethanol, v/v). The radioactivity of beads in the tubes was measured with a well-type γ-counter (1480 Wizard3, PerkinElmer Japan Co., Osaka, Japan). Binding ratios were calculated as (radioactivity of beads)/(total applied radioactivity)/(protein abundance on beads) x 100 (% dose/μg protein).

For cell uptake studies, medium from 24-well plates in which differentiated adipocytes or undifferentiated 3T3-L1 cells were cultured was removed. After washing with PBS(-), 0.5 ml BMS309403 in DMEM (0-10 μM, 1% DMSO, v/v) was added and incubated at 37 °C for 1 hr. Then, 0.05 ml [^{18}F]FTAP1 (0.22 MBq, 1% DMSO and 0.1 % Tween 20, v/v) was added and incubated at 37 °C for 1 hr. After washing with 0.5 ml PBS(-) (1% DMSO and 0.1 % Tween 20, v/v) three times, the cells were lysed with 0.25 ml 2N NaOH for radioactivity and protein content measurements. Binding ratios were calculated as: (radioactivity in collected cells)/(total applied radioactivity)/(protein abundance) x 100 (% dose/mg protein).

The [^{18}F]FTAP1 partition coefficient was measured with 1-octanol and phosphate buffer at pH 7.4. The two phases were pre-saturated, and a mixture of 3.0 ml 1-octanol and 3.0 ml PBS(-) was added to a tube containing 0.02 ml [^{18}F]FTAP1 in PBS(-) (0.16 MBq, 5% DMSO, v/v). The test tube was vortexed and centrifuged (1,000 x *g*, 5 min).

Aliquots from the 1-octanol and buffer phases (0.5 ml) were counted with a well-type γ-counter. This procedure was repeated three times. The partition coefficient was calculated from the ratio of radioactivity in the organic and aqueous layers.

The *in vitro* stability of [^{18}F]FTAP1 in plasma was measured using plasma samples taken from ddY mice (males, 7 weeks old). After addition of 0.01 ml [^{18}F]FTAP1 (0.08 MBq, 5% DMSO, v/v) to 0.1 ml plasma, the mixture was incubated at 37 °C for 2 hr. After addition of 0.2 ml methanol and vortexing, the mixture was centrifuged (4,160 x *g*, 10 min). The supernatant was filtered with a low protein binding hydrophilic PTFE membrane (Millex-LH MILLIPORE), and the filtrate was analyzed by RP-HPLC using a Cosmosil C18 column (5C18-AR-II, 10 mm x 250 mm, CH_3CN/water = 50/50 (0 min)-70/30 (40 min); flow rate = 1.5 ml/min).

The serum protein binding ratio of [^{18}F]FTAP1 was measured using rapid equilibrium dialysis (RED) devices (Thermo Fisher Scientific K.K.) following the manufacturer's procedures. Briefly, 0.02 ml [^{18}F]FTAP1 (0.43 MBq, 5% ethanol, v/v) and mouse plasma (0.3 ml) were mixed and placed in the sample chamber with 0.5 ml PBS (-) added to the RED device buffer chamber. After incubation at 37 °C for 4 hr, 0.05 ml of the samples were obtained from each chamber. The binding ratios were calculated as: (sample chamber radioactivity)-(buffer chamber radioactivity)/(sample chamber radioactivity) x

100 (%).

7. In vivo and ex vivo evaluations of [^{18}F]FTAP1

A saline solution of [^{18}F]FTAP1 (0.07-0.10 MBq, 0.1% Tween 20, v/v) was injected intravenously into a lateral tail vein of C6 cell implantation model mice (males, 8 weeks old). The mice were sacrificed at various post-injection time points, and the organs of interest, including tumor tissues, were removed. The organ weights were determined, and the radioactivity in the organs was measured with a well-type γ-counter. Several tumor model mice were sacrificed 3 hr after the probe injection by transcardial perfusion of saline (20 ml) under anesthesia. The weight and radioactivity of the removed organs, including tumor tissues, were measured as mentioned above.

The tumors were removed for metabolite analysis 3 hr after intravenous injection of a saline solution including [^{18}F]FTAP1 (185 MBq, 0.1% Tween 20, v/v) in tumor bearing mice and homogenized in 1 ml ice-cold 30 mM Tris-HCl buffer (pH = 8.5) containing 5 mM magnesium acetate at 4 °C. After addition of 3 ml cold methanol and vortexing, tissue samples were centrifuged (10,000 x *g*, 5 min). The supernatants were filtered, and the filtrate was analyzed by RP-HPLC as described above.

The tumors removed 3 hr after injection of [^{18}F]FTAP1 (81 MBq) were also subjected

to *ex vivo* autoradiography and immunohistochemistry. Ten μm thick sections of the tumor were prepared with a cryomicrotome (CM1900, Leica Microsystems) and exposed to imaging plates (BAS-SR, Fuji Photo Film) for 2 hr. Autoradiograms of these sections were obtained with a BAS5000 scanner (Fuji Photo Film). The adjacent sections were subjected to immunohistochemical staining for FABP4 and perilipin, an adipocyte marker, with hematoxylin counterstaining performed as described in our previous report [9]. A FABP4–specific polyclonal rabbit IgG (ab13979, Abcam) and a perilipin–specific monoclonal rabbit IgG (D1D8, Cell Signaling) were used as the primary antibodies. Antibodies from the Dako Envision + kit (K4002, Dako) were used as secondary antibodies for both primary antibodies. Subclass-matched irrelevant IgG served as a negative control.

Dynamic small-animal PET/computed tomography (CT) scans were performed with [^{18}F]FTAP1 in tumor-bearing mice. The body temperature was maintained using a heating pad throughout the procedure. [^{18}F]FTAP1 (37 MBq, 0.1% tween 20, v/v) was intravenously injected into mice, followed by PET scanning acquired over 172–202 min (5 min/frame) under isoflurane anesthesia (2.5% in an air mixture). CT scans were performed for anatomic reference (spatial resolution, 50 μm; 60 kV; and 310 μA). PET and CT images were reconstructed using three-dimensional ordered-subset expectation

maximization and a modified three-dimensional cone-beam Feldkamp algorithm resulting in a 0.177- x 0.177- x 0.177-mm voxel size for a 512 x 512 x 512 image volume, respectively. Acquired images were processed with PMOD Biomedical Image Quantification (PMOD Technologies, Ltd.).

8. Statistical analysis

The Ki values are expressed as mean ± standard errors of the means (SEM), while the other data are expressed as mean ± SD. Statistical analysis was performed with the Mann-Whitney *U* test. *P* values < 0.05 were considered statistically significant.

Results

1. In vitro evaluation of nonradioactive compounds and radiosynthesis

A competitive binding assay using the established FABP4 ligand, 1,8-ANS, revealed the affinity of FTAP1 and FTAP3 for FABP4. Analysis of inhibition curves allowed determination of K_i values of 68 ± 8.9 and 490 ± 41 nM for FTAP1 and FTAP3, respectively. The membrane permeability determined by a PAMPA plate system was 1.5 ± 0.3 x 10^{-6} and 0.18 ± 0.08 x 10^{-6} cm/s for FTAP1 and FTAP3, respectively.

Based on the results of these evaluations, FTAP1 was chosen for further experiments. [^{18}F]FTAP1 was successfully synthesized following the scheme shown in Fig. 2. The radiochemical yield was 31 ± 17%, and the radiochemical purity was above 98% after purification by RP-HPLC.

2. In vitro evaluation of [^{18}F]FTAP1

The selectivity assay of [^{18}F]FTAP1 binding to FABP4 compared with that to FABP3 and FABP5 (Fig. 3) using each immobilized protein revealed that [^{18}F]FTAP1 binding to FABP4 was 16.3-fold higher than to FABP3 and 9.3-fold higher than to FABP5 (6.7 ± 3.6% dose/μg protein (FABP4) vs. 0.4 ± 0.7% dose/μg protein (FABP3) and 0.7 ± 0.4% dose/μg protein (FABP5), $P < 0.05$).

Cellular uptake of [^{18}F]FTAP1 into adipocytes and 3T3-L1 preadipocytes was evaluated to clarify whether [^{18}F]FTAP1 binds to intracellular FABP4 (Fig. 4). Cell differentiation and FABP4 expression in differentiated adipocytes were confirmed by Oil red O staining and western blot analysis, respectively, in a similar way to that described in our previous report [9]. [^{18}F]FTAP1 showed significantly higher radioactivity in adipocytes than 3T3-L1 preadipocytes. Furthermore, the radioactivity accumulation in adipocytes was significantly and dose-dependently inhibited by treatment with the FABP4-specific inhibitor BMS309403, which at 10 μM inhibited almost all (ca. 95%) of the total probe uptake.

The partition coefficient (a log*P* value) of [^{18}F]FTAP1 was estimated to be 1.7 ± 0.04. Over 95% of radioactivity was observed in an intact form by HPLC analysis after 2 hr incubation in mouse plasma at 37 °C, which indicates the high stability of [^{18}F]FTAP1. The percentage of [^{18}F]FTAP1 bound to serum proteins was found to be more than 99%.

3. In vivo and ex vivo evaluations of [^{18}F]FTAP1

Table 1 shows the biodistribution of [^{18}F]FTAP1 in C6 tumor bearing mice. [^{18}F]FTAP1 was cleared through excretion via the liver and kidneys while low-level radioactivity was observed in the bones, suggesting that [^{18}F]FTAP1 was resistant to

defluorination *in vivo*. [^{18}F]FTAP1 showed moderate radioactivity accumulation in tumors, which peaked 180 min after injection (3.86 ± 0.39 % ID/g). The tumor to muscle ratio of radioactivity accumulation increased in a time-dependent manner and reached 4.5 at 180 min after probe injection. Considering the high radioactivity retention in circulating blood, the influence of blood radioactivity on the radioactivity remaining in the tumors was evaluated by comparing the radioactivity accumulation in tumor tissues of mice sacrificed by decapitation and transcardial perfusion. While the lung radioactivity was reduced by 90%, there was no difference in tumor accumulations, with the radioactivity accumulations in tumors and lungs in mice sacrificed by decapitation being 3.86 and 5.45 % ID/g, respectively, while those in mice sacrificed by transcardial perfusion were 4.14 and 0.51 % ID/g, respectively.

The radioactive chemical composition in tumors 3 hr after [^{18}F]FTAP1 administration was analyzed by RP-HPLC of excised tumor homogenates (Fig. 5). In tumors (Fig. 5B), no distinct metabolite peaks were observed and the retention time of an observed main peak was the same as that for [^{18}F]FTAP1 (Fig. 5A). These results indicate that [^{18}F]FTAP1 exists in an intact form in tumors.

Ex vivo autoradiographic analysis (Fig. 6A) showed a heterogeneous radioactivity distribution in tumor sections 3 hr after [^{18}F]FTAP1 injection, and the accumulation

profile essentially corresponded to FABP4-positive areas (Fig. 6A and B, black arrow). The expression of perilipin, an adipocyte marker, was also confirmed in FABP4-positive areas (Fig. 6C).

Finally, PET/CT imaging of tumor-bearing mice was performed 3 hr after [^{18}F]FTAP1 injection. As shown in Fig. 7, the tumor in the right hind legs was visualized, while the bladder exhibited high radioactivity due to probe excretion.

Discussion

In the present study we developed [^{18}F]FTAP1 for *in vivo* PET imaging of FABP4, which is closely related to CAA functions [5], tumor progression [5], and atherosclerotic plaque instability [13]. This probe is based on our previous radioiodinated probe, [$^{123/125}$I]TAP1 [9]. [^{18}F]FTAP1 showed high affinity and selectivity for FABP4, adequate cellular membrane permeability, and high uptake into differentiated adipocytes expressing FABP4 that could be perfectly blocked by a selective FABP4 inhibitor. [^{18}F]FTAP1 time-dependently accumulated in an intact form in C6 implanted tumors, which enabled *in vivo* tumor imaging with a PET/CT scanner designed for use with small animals. Furthermore, the regional radioactivity distribution corresponding to the FABP4 expression profile in tumor sections was confirmed. Together, these results indicate that [^{18}F]FTAP1 is a promising imaging probe that targets FABP4.

We recently developed and evaluated a novel radioiodinated probe, [$^{123/125}$I]TAP1, as a FABP4 imaging probe [9]. The design of [^{125}I]TAP1 was based on the structures of several FABP4 inhibitors, and *in vitro* results showed superior affinity and selectivity for FABP4. However, this probe was highly lipophilic, which led to significant nonspecific accumulation *in vitro* and *in vivo*, and caused difficulties for *in vivo* imaging. As such, this high lipophilicity was considered to be a critical drawback of [^{125}I]TAP1. In this study,

we aimed to reduce the lipophilicity of the FABP4-specific probe for optimization of *in vivo* imaging while maintaining the superior characteristics of the original probe. To design a probe that has reasonable lipophilicity and membrane permeability so that delivery to intracellular target molecules (e.g. FABP4) can be achieved after derivatization, we adopted two strategies: 1) substitution of radiofluorine for radioiodine as the labeling radionuclide, and 2) introduction of short oxyethylene linkers between the radionuclide and the core probe structure. The introduction of a longer oxyethylene linker (FTAP3) excessively diminished membrane permeability and also reduced binding affinity to FABP4, probably because of the additional steric hindrance exerted on the interaction of FTAP3 with the FABP4 protein. On the other hand, use of a shorter linker (single oxyethylene linker) in [^{18}F]FTAP1 successfully provided reasonable lipophilicity (the log*P* values of [^{18}F]FTAP1 and [^{125}I]TAP1 were 1.7 ± 0.04 and 2.7 ± 0.1, respectively) and adequate membrane permeability for intracellular targeting [14], while retaining a high binding affinity for FABP4. Our results are supported by the previous report that investigated the correlation between cell permeability and biophysical properties of the compound, including log*P* values and molecular weight [15]. Furthermore, almost all [^{18}F]FTAP1 accumulation in adipocytes was inhibited by treatment with the FABP4 inhibitor 10 μM BMS309403, indicating a successful reduction

in nonspecific accumulation, compared with radioiodinated TAP1 that showed ~50% nonspecific accumulation in the same experimental setting [9]. Thus, as expected, [^{18}F]FTAP1 was successfully derived and had a low nonspecific accumulation while maintaining FABP4 binding capacity.

The biodistribution study in tumor bearing mice also revealed a superior property of [^{18}F]FTAP1 as compared to [^{125}I]TAP1. Namely, tumor accumulations were 3.9 % dose/g and 2.3 % dose/g for [^{18}F]FTAP1 and [^{125}I]TAP1, respectively, while the tumor to muscle ratios were 4.5 and 3.6 for [^{18}F]FTAP1 and [^{125}I]TAP1, respectively. The background signal might be increased if a blood fraction exists in tumor tissues because circulating blood showed somewhat high radioactivity levels. However, the finding that tumors taken from mice sacrificed by transcardial perfusion showed comparable radioactivity levels to those taken from mice sacrificed by decapitation clearly indicates that the influence of residual blood radioactivity on tumor accumulation was low. For future applications, high radioactivity remaining in circulating blood could present an obstacle to accurate imaging. Since the remaining radioactivity might be due to the high protein binding of [^{18}F]FTAP1, a detailed analysis of the interaction between the probe and serum proteins such as albumin and acidic glycoprotein would provide information on how this possible background effect could be reduced. In any case, PET/CT imaging using [^{18}F]FTAP1 was

successful in visualizing C6 cells implanted tumors in living mice, which is consistent with the biodistribution study described above. A ring-shaped radioactivity accumulation profile observed in the tumor region in PET images might reflect adipocytes that surround the tumor and express FABP4, as was indicated in the immunohistochemical results.

Recently, the role of CAA in tumor progression has been gathering attention. Nieman *et al*. [5] reported that CAAs metabolically interact with SKOV3ip1 cells and promote fatty acid metabolism in these cells that is required for proliferation. They also revealed that this interaction could be inhibited by a FABP4 inhibitor, and that the expression of FABP4 in tumor cells in the boundary areas between tumor cells and CAAs is enhanced. Thus, FABP4 could be a key participant in the metabolic interaction between these cells. Different tumor cells have been reported to express varying levels of FABP4, while some lack this protein [16-18]. Since FABP4 is not expressed in C6 cells *in vitro* [9] but expressed in human glioblastoma lesion *in vivo* [16], we used C6 cell line as a model system leading to increased FABP4 expression in CAAs surrounding C6 tumors to evaluate FABP4 targeting probes *in vivo*. In this study, FABP4 is only expressed in CAAs surrounding tumors and [^{18}F]FTAP1 detects them. FABP4 expressed in tumor stromal cells is reported to be related to glioma malignancy [16], suggesting that FABP4 imaging with [^{18}F]FTAP1 could be useful for evaluating the potential for glioma malignancy. On

the other hand, in other tumors, including bladder cancers, FABP4 is reported to be expressed in tumor cells and is related to the disease pathology [17, 18]. FABP4 expressed in macrophages is also reported to correlate with instability of atherosclerotic plaques [13]. Thus, FABP4 imaging could be useful not only for evaluating the detailed functions of FABP4 in multiple settings and for the development of therapeutic agents that target FABP4, but also for assessing the pathophysiological grades of related diseases.

In conclusion, we developed a novel radiofluorinated probe, [^{18}F]FTAP1, for *in vivo* PET imaging of FABP4 that is closely related to various pathologies in cancers. [^{18}F]FTAP1 demonstrated superior *in vitro* and *in vivo* characteristics with low non-specific binding and succeeded in PET imaging of xenografted tumors. These findings indicate that [^{18}F]FTAP1 is a promising PET probe that targets FABP4.

Acknowledgment:

The authors have no competing interest to declare. This work was supported in part by a Health and Labour Science Research Grant “Research on Noninvasive and Minimally Invasive Medical Devices” from the Ministry of Health, Labour and Welfare of Japan and by JSPS KAKENHI Grant Number 24591813. The funders had no role in study design, data collection and analysis, decision to publish, or preparation of the manuscript.

References

[1] Finucane MM, Stevens GA, Cowan MJ, Danaei G, Lin JK, Paciorek CJ, et al. National, regional, and global trends in body-mass index since 1980: systematic analysis of health examination surveys and epidemiological studies with 960 country-years and 9.1 million participants. Lancet 2011;377:557-67.

[2] Renehan AG, Tyson M, Egger M, Heller RF, and Zwahlen M. Body-mass index and incidence of cancer: a systematic review and meta-analysis of prospective observational studies. Lancet 2008;371:569-78.

[3] Hefetz-Sela S and Scherer PE. Adipocytes: impact on tumor growth and potential sites for therapeutic intervention. Pharmacology & therapeutics 2013;138:197-210.

[4] Dirat B, Bochet L, Dabek M, Daviaud D, Dauvillier S, Majed B, et al. Cancer-associated adipocytes exhibit an activated phenotype and contribute to breast cancer invasion. Cancer research 2011;71:2455-65.

[5] Nieman KM, Kenny HA, Penicka CV, Ladanyi A, Buell-Gutbrod R, Zillhardt MR, et al. Adipocytes promote ovarian cancer metastasis and provide energy for rapid tumor growth. Nature medicine 2011;17:1498-503.

[6] Furuhashi M and Hotamisligil GS. Fatty acid-binding proteins: role in metabolic diseases and potential as drug targets. Nature reviews. Drug discovery 2008;7:489-503.

[7] Shen WJ, Sridhar K, Bernlohr DA, and Kraemer FB. Interaction of rat hormone-sensitive lipase with adipocyte lipid-binding protein. Proceedings of the National Academy of Sciences of the United States of America 1999;96:5528-32.

[8] Makowski L and Hotamisligil GS. Fatty acid binding proteins--the evolutionary crossroads of inflammatory and metabolic responses. The Journal of nutrition 2004;134:2464S-8S.

[9] Nishigori K, Temma T, Onoe S, Sampei S, Kimura I, Ono M, et al. Development of a radioiodinated triazolopyrimidine probe for nuclear medical imaging of Fatty Acid binding protein 4. PLoS One 2014;9:e94668.

[10] Kimura I, Ozawa K, Inoue D, Imamura T, Kimura K, Maeda T, et al. The gut microbiota suppresses insulin-mediated fat accumulation via the short-chain fatty acid receptor GPR43. Nature communications 2013;4:1829.

[11] Kakwani MD, Palsule Desai NH, Lele AC, Ray M, Rajan MG, and Degani MS. Synthesis and preliminary biological evaluation of novel N-(3-aryl-1,2,4-triazol-5-yl) cinnamamide derivatives as potential antimycobacterial agents: an operational Topliss Tree approach. Bioorganic & medicinal chemistry letters 2011;21:6523-6.

[12] Kane CD and Bernlohr DA. A simple assay for intracellular lipid-binding proteins using displacement of 1-anilinonaphthalene 8-sulfonic acid. Analytical biochemistry

1996;233:197-204.

[13] Agardh HE, Folkersen L, Ekstrand J, Marcus D, Swedenborg J, Hedin U, et al. Expression of fatty acid-binding protein 4/aP2 is correlated with plaque instability in carotid atherosclerosis. Journal of internal medicine 2011;269:200-10.

[14] Avdeef A. Physicochemical profiling (solubility, permeability and charge state). Current topics in medicinal chemistry 2001;1:277-351.

[15] Camenisch G, Alsenz J, van de Waterbeemd H, and Folkers G. Estimation of permeability by passive diffusion through Caco-2 cell monolayers using the drugs' lipophilicity and molecular weight. European journal of pharmaceutical sciences : official journal of the European Federation for Pharmaceutical Sciences 1998;6:317-24.

[16] Cataltepe O, Arikan MC, Ghelfi E, Karaaslan C, Ozsurekci Y, Dresser K, et al. Fatty acid binding protein 4 is expressed in distinct endothelial and non-endothelial cell populations in glioblastoma. Neuropathology and applied neurobiology 2012;38:400-10.

[17] Boiteux G, Lascombe I, Roche E, Plissonnier ML, Clairotte A, Bittard H, et al. A-FABP, a candidate progression marker of human transitional cell carcinoma of the bladder, is differentially regulated by PPAR in urothelial cancer cells. International journal of cancer. Journal international du cancer 2009;124:1820-8.

[18] Tolle A, Suhail S, Jung M, Jung K, and Stephan C. Fatty acid binding proteins

(FABPs) in prostate, bladder and kidney cancer cell lines and the use of IL-FABP as survival predictor in patients with renal cell carcinoma. BMC cancer 2011;11:302.

Table 1. Radioactivity biodistribution after intravenous administration of [^{18}F]FTAP1 in C6 bearing mice.

	Time after administration (min)				
	5	30	60	120	180
Blood	22.27 ± 1.54	15.29 ± 1.92	12.44 ± 1.43	10.12 ± 0.44	10.38 ± 0.56
Heart	4.56 ± 0.48	4.55 ± 0.47	3.64 ± 0.56	3.03 ± 0.20	2.88 ± 0.50
Lung	12.74 ± 1.58	10.56 ± 1.52	6.11 ± 1.13	5.45 ± 1.03	5.71 ± 0.77
Liver	36.32 ± 1.72	31.89 ± 2.65	25.59 ± 4.65	20.50 ± 2.28	17.63 ± 1.08
Kidney	31.94 ± 6.70	24.42 ± 2.81	20.84 ± 2.99	17.14 ± 2.16	15.19 ± 2.12
Intestine	17.65 ± 13.11	6.57 ± 0.80	9.96 ± 1.14	13.39 ± 0.37	19.24 ± 3.49
Stomach[a]	0.54 ± 0.10	0.63 ± 0.10	0.72 ± 0.20	0.97 ± 0.15	0.73 ± 0.32
Spleen	2.93 ± 0.15	1.96 ± 0.20	1.87 ± 0.08	1.33 ± 0.11	1.55 ± 0.29
Pancreas	2.66 ± 0.30	2.13 ± 0.08	1.70± 0.30	1.36± 0.18	1.26 ± 0.10
Muscle	0.78 ± 0.16	0.96 ± 0.15	1.03 ± 0.21	0.98 ± 0.02	0.88 ± 0.13
Bone	1.45 ± 0.23	1.44 ± 0.14	1.49 ± 0.32	1.28 ± 0.10	1.95 ± 0.58
Brain	0.36 ± 0.06	0.26 ± 0.04	0.25 ± 0.04	0.20 ± 0.02	0.24 ± 0.01
Tumor	1.13 ± 0.22	2.48 ± 0.54	2.96 ± 0.16	3.74 ± 0.31	3.86 ± 0.39
Tumor/Muscle	1.45 ± 0.15	2.57 ± 0.30	2.95± 0.57	3.83 ± 0.28	4.49 ± 0.90
Tumor/Blood	0.05 ± 0.01	0.16 ± 0.02	0.24± 0.02	0.36 ± 0.04	0.37 ± 0.05

Data are presented as % injected dose per gram. Each value represents the mean ± s.d. for 3 animals at each interval. [a] Presented as % injected dose per organ.

Figure Legends

Fig. 1

Synthesis of nonradioactive FTAP1 (***3***), nonradioactive FTAP3 (***6***), and FTAP1 precursor (***10***).

Fig. 2

Radiosynthesis of [^{18}F]FTAP1.

Fig. 3

Binding of [^{18}F]FTAP1 to the FABP3, 4, and 5 analogues. $^{*}P < 0.05$ vs. FABP4 group.

Fig. 4.

Uptake of [^{18}F]FTAP1 into adipocytes and 3T3-L1 cells, and inhibition by BMS309403. $^{\#}P < 0.05$ vs. 3T3-L1 group, $^{\dagger}P < 0.05$ vs. 1 μM group, $^{\S}P < 0.05$ vs. 10 μM group.

Fig. 5.

Analysis of [^{18}F]FTAP1 in saline (A) and of tumor homogenates at 180 min after intravenous injection of [^{18}F]FTAP1 (B).

Fig. 6.

Regional distribution determined by autoradiography of radioactivity 180 min after the injection of [^{18}F]FTAP1 (A). FABP4 and perilipin immunohistochemical staining of sections adjacent to A (B, C). Bar = 1 mm (B, C).

Fig. 7.

PET/CT imaging 180 min after [^{18}F]FTAP1 injection into C6 bearing mice.

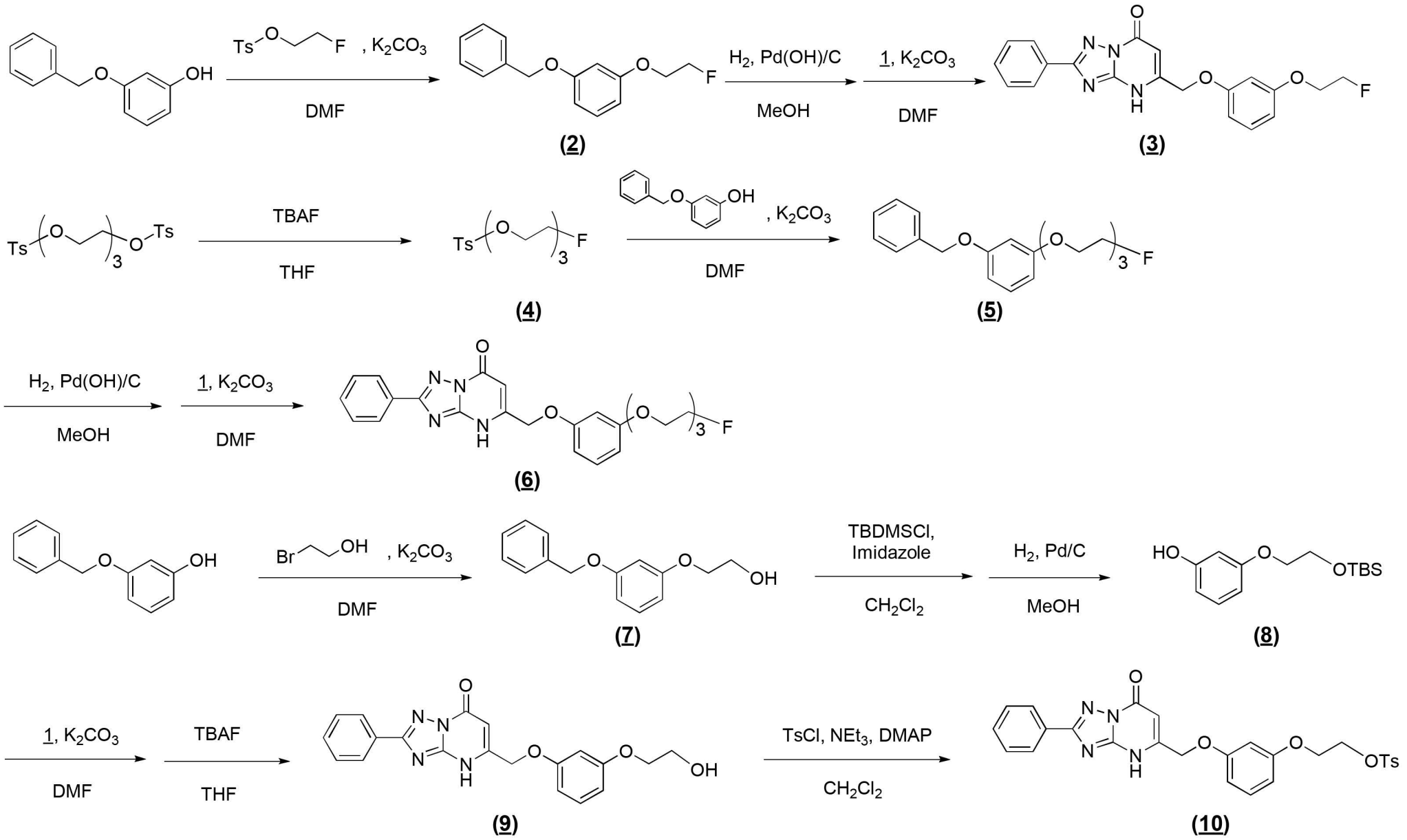
Ts
O
F
, K_2CO_3
DMF
OH
(2)
H_2, Pd(OH)/C
MeOH
1, K_2CO_3
DMF
(3)
TBAF
THF
(4)
(5)
(6)
Br
(7)
TBDMSCl,
Imidazole
CH_2Cl_2
HO
OTBS
(8)
TsCl, NEt_3, DMAP
OTs
(9)
(10)

Fig. 1

Fig. 2

Fig. 3

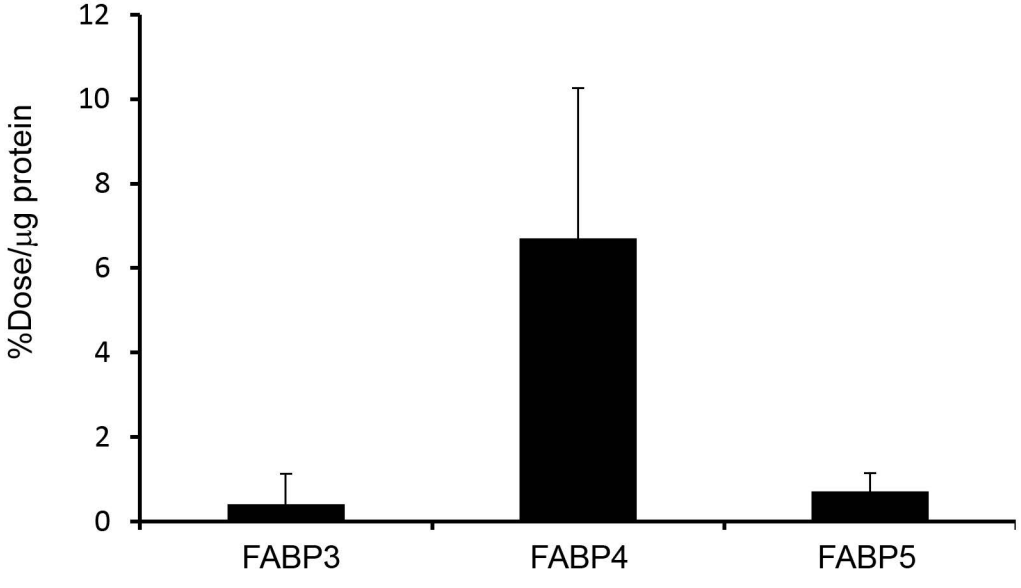

Fig. 4

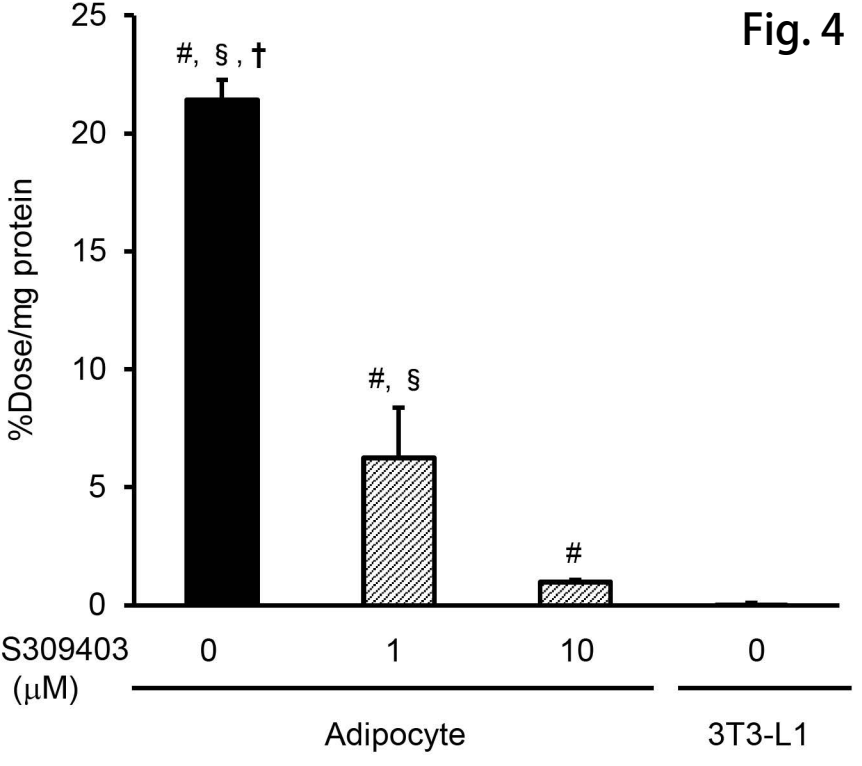
25
20
15
10
5
0
%Dose/mg protein
#, §, †
#, §
#
BMS309403
(μM)
0
1
10
0
Adipocyte
3T3-L1

Fig. 5

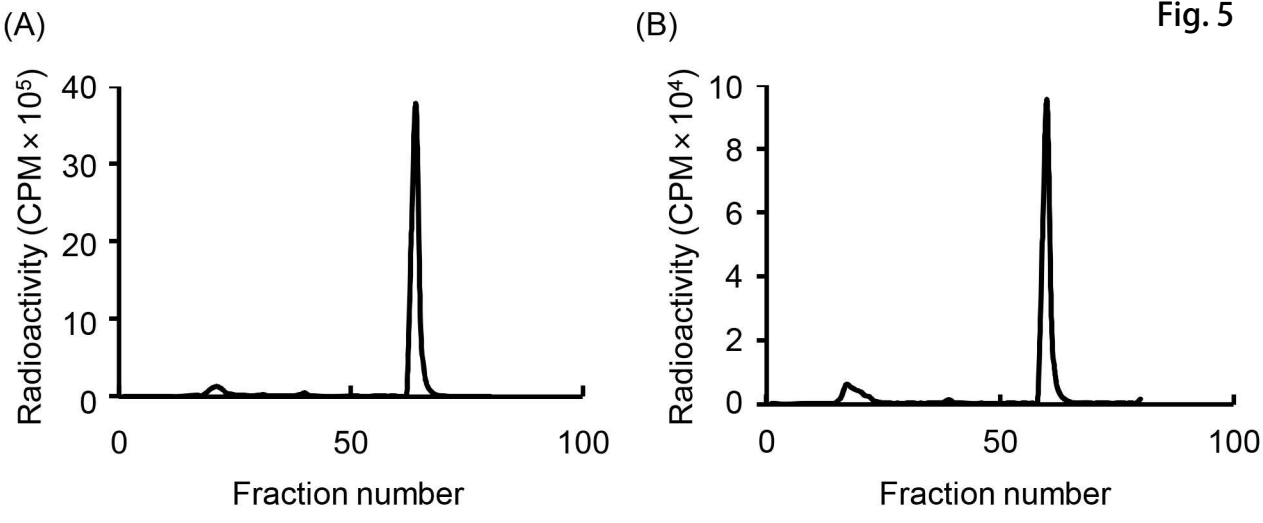
(A)
Radioactivity (CPM × 10^5)
40
30
20
10
0
0
50
100
Fraction number
(B)
Radioactivity (CPM × 10^4)
10
8
6
4
2
0
0
50
100
Fraction number

Fig. 6

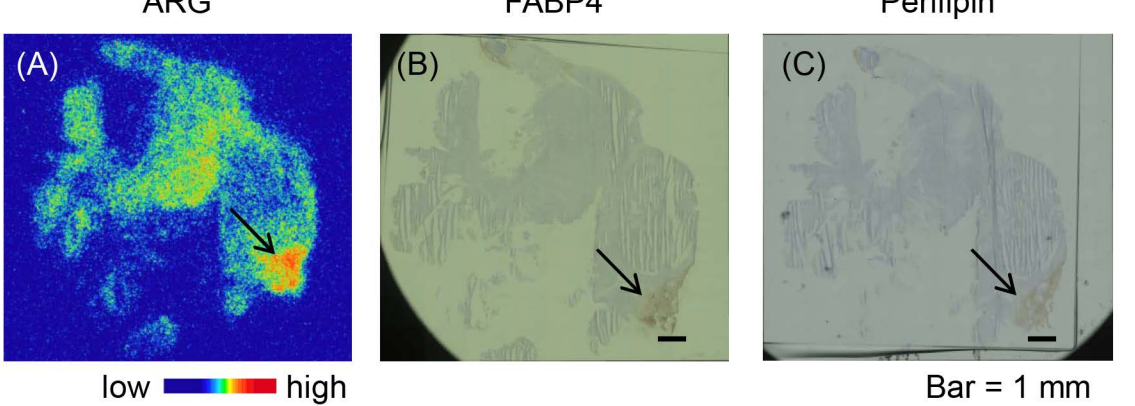

Fig. 7

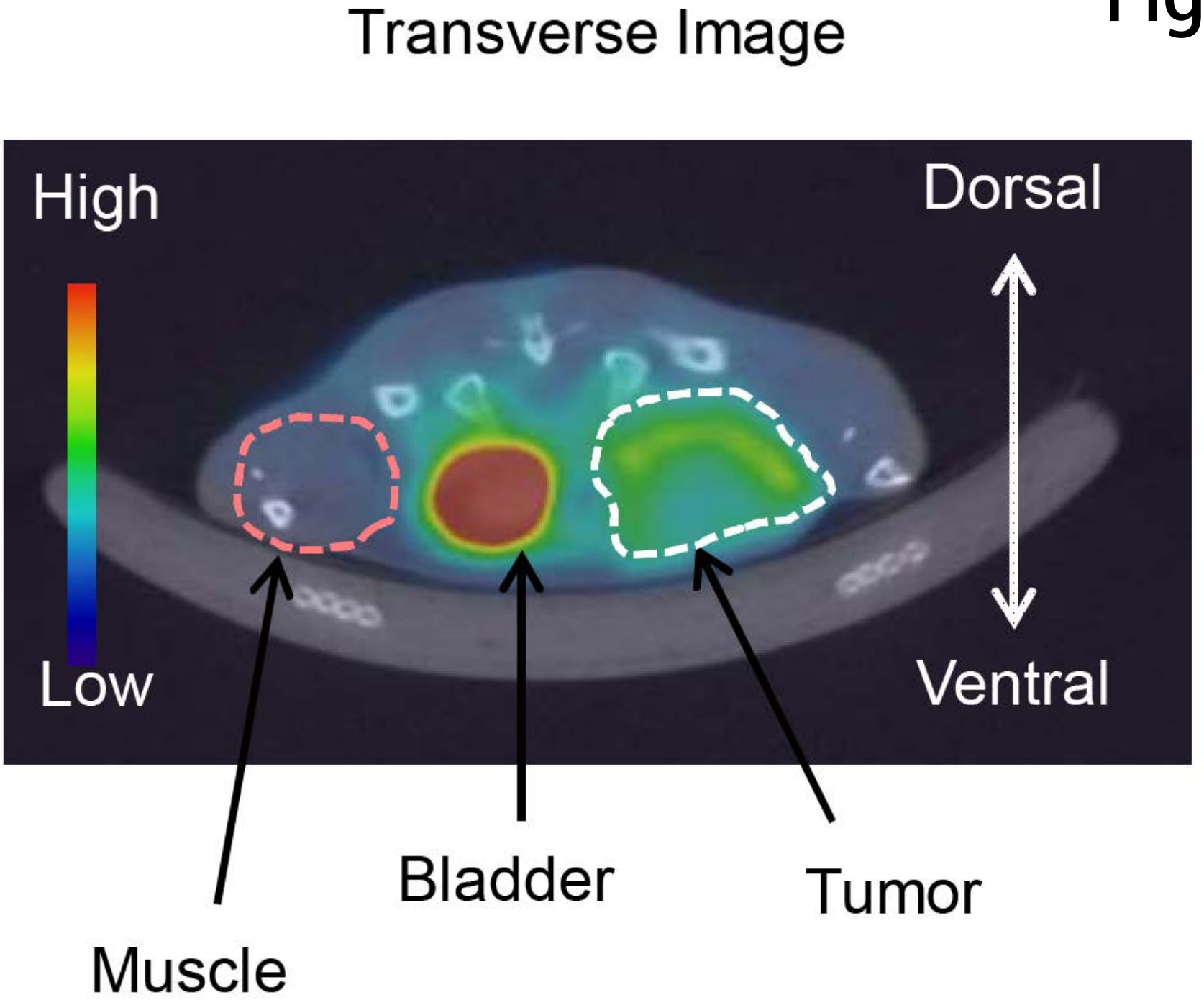
Transverse Image
High
Low
Dorsal
Ventral
Muscle
Bladder
Tumor